Direct Free Energy Evaluation of Classical and Quantum Many-Body Systems via Field-Theoretic Simulation

Glenn H. Fredrickson[a,1] **and Kris T. Delaney**[b]

[a]Departments of Chemical Engineering and Materials, Materials Research Laboratory, University of California at Santa Barbara, Santa Barbara, CA 93106; [b]Materials Research Laboratory, University of California at Santa Barbara, Santa Barbara, CA 93106

This manuscript was compiled on July 5, 2022

Free energy evaluation in molecular simulations of both classical and quantum systems is computationally intensive and requires sophisticated algorithms. This is because free energy depends on the volume of accessible phase space, a quantity that is inextricably linked to the integration measure in a coordinate representation of a many-body problem. In contrast, the same problem expressed as a field theory (auxiliary field or coherent states) isolates the particle number as a simple parameter in the Hamiltonian or action functional and enables the identification of a chemical potential field operator. We show that this feature leads a new "direct" method of free energy evaluation in which a particle model is converted to a field theory and appropriate field operators averaged using a field-theoretic simulation conducted with complex Langevin sampling. These averages provide an immediate estimate of the Helmholtz free energy in the canonical ensemble and the entropy in the microcanonical ensemble. The method is illustrated for a classical polymer solution, a block copolymer melt exhibiting liquid crystalline and solid mesophases, and a quantum fluid of interacting bosons.

molecular simulation | free energy | field theory | field-theoretic simulation | polymers | quantum fluids | complex Langevin

Free energy evaluation is notoriously difficult in molecular simulations, involving laborious procedures such as thermodynamic integration, particle insertion, histogram reweighting, and acceptance ratios (1–4). Because free energy reflects the volume of accessible phase space in the ensemble of interest, there is no simple operator in coordinate representations of classical and quantum many-body systems that can be averaged to obtain a free energy. The closest such operator is the object averaged during Widom test particle insertion to estimate the chemical potential of a fluid (5). However, extensions of the Widom method to polymeric fluids show reduced efficiency with increasing density and chain length (6–9), melts of high molecular weight polymers being a particularly challenging case. The celebrated Wang-Landau algorithm has significantly simplified free energy calculations based on Monte Carlo sampling for both classical (10, 11) and quantum systems (12). Nonetheless, free energy estimation by such flat histogram methods remains a multi-step procedure that relies on sophisticated algorithms and, in the quantum Monte Carlo case, high temperature or other perturbation expansions.

Classical fluids. It is not broadly appreciated that the partition function for a classical fluid or polymer model with soft-core pair interactions can be exactly converted into a statistical field theory. This proceeds by separating attractive and repulsive non-bonded interactions and applying Hubbard-Stratonovich transforms (13, 14). Such field theories contain one or more *auxiliary fields* (AF) that serve to decouple the non-bonded interactions in the system, facilitating a reduction to a single-molecule statistical mechanics problem. As a simple example, a monatomic fluid with interactions described by a pair potential $u(r)$ has a canonical partition function given by (15)

$$\mathcal{Z}(n,V,T) = \frac{1}{n!\lambda_T^{3n}} \int d^{3n}r \; \exp\left(-\beta \sum_{j<k} u(r_{jk})\right) \qquad [1]$$

where n is the number of atoms, $\beta \equiv 1/(k_B T)$ the inverse of the thermal energy, k_B the Boltzmann constant, and λ_T the thermal de Broglie wavelength. The sum in this expression is over all pairs of atoms j, k, and $r_{jk} \equiv |\mathbf{r}_j - \mathbf{r}_k|$ is the distance between the pair. The integral extends over all $3n$ coordinates of the particles within the system volume V. For potentials $u(r)$ that are finite on contact and positive definite (purely repulsive), Eq. 1 can be equivalently expressed as an AF-type field theory of the form (14)

$$\mathcal{Z}(n,V,T) = \mathcal{Z}_0 \int \mathcal{D}w \; \exp\left(-H[w]\right) \qquad [2]$$

where $\mathcal{Z}_0$ contains the ideal-gas partition function and an n-independent normalizing factor (see the Supplementary Information Appendix, SI). The functional integral in this expression extends over all realizations of the real auxiliary field $w(\mathbf{r})$ with points $\mathbf{r}$ spanning the system volume. $H[w]$ is a

Significance Statement

The accurate evaluation of free energies within molecular simulations is important to many scientific fields including fluid and solid phase equilibria, biomolecular condensates, and quantum phase transitions, among others. Unfortunately, free energy estimation is tedious and computationally expensive for molecular models whose degrees of freedom are expressed in particle coordinates. We show that alternative representations of a model as a classical or quantum field theory provide access to a chemical potential operator that can be averaged to yield a direct and low-cost estimate of the Gibbs free energy. The averaging is performed using a "field-theoretic" computer simulation that employs fluctuating fields rather than particles.

G.H.F. and K.T.D. jointly conceived this work and G.H.F. prepared the manuscript. K.T.D. wrote the software, implemented the algorithms described, and produced the figures.

The authors declare no competing interests.

[1]To whom correspondence should be addressed. E-mail: ghf@ucsb.edu, kdelaney@mrl.ucsb.edu

Hamiltonian functional given by

$$H[w] = \frac{1}{2\beta}\int_V d^3r \int_V d^3r'\; w(\mathbf{r})u^{-1}(|\mathbf{r}-\mathbf{r}'|)w(\mathbf{r}') - n\ln Q[iw] \qquad [3]$$

with $u^{-1}(r)$ the functional inverse of the pair potential and $Q[iw] \equiv (1/V)\int_V d^3r\; \exp[-iw(\mathbf{r})]$ the partition function of a *single atom* experiencing a purely imaginary potential $iw(\mathbf{r})$, with $i \equiv \sqrt{-1}$.

Equations 1 and 2 are mathematically equivalent representations of the same molecular model, but have dramatically different forms. The conventional coordinate representation of Eq. 1 has the particle number n intractably embedded in the integration measure, while n enters the field-theoretic representation Eq. 2 through the ideal gas term $\mathcal{Z}_0$ and as an explicit factor in the final contribution to $H[w]$. In the coordinate representation, it is not possible to evaluate the chemical potential by the thermodynamic expression $\mu = (\partial A/\partial n)_{V,T}$ with $A \equiv -k_BT\ln\mathcal{Z}$ the Helmholtz free energy, so there is no simple chemical potential operator. In contrast, within the AF representation the same derivative yields

$$\beta\mu = \beta\mu_0 - \frac{\int \mathcal{D}w\; \ln Q[iw]\exp(-H[w])}{\int \mathcal{D}w\; \exp(-H[w])} \equiv \beta\mu_0 - \langle \ln Q[iw]\rangle \qquad [4]$$

where μ_0 is the ideal gas chemical potential and $\langle\cdots\rangle$ denotes an ensemble average in the field theory. A "field operator" for the excess chemical potential $\mu_{\rm ex}$ is thus identified as $\tilde{\mu}_{\rm ex}[w] \equiv -k_BT\ln Q[iw]$, a functional whose ensemble average is $\mu_{\rm ex}$. A similar field operator for the pressure, $\tilde{P}[w]$, is provided in Eq. S15 of the SI. It is derived by scaling the coordinate system to unit volume, forming the derivative $P = -(\partial A/\partial V)_{n,T}$, and then restoring the original volume scaling (16, 17).

This difference in analytic structure between coordinate and field representations of molecular models greatly simplifies free energy estimation in the latter. For example, in a fluid phase within the canonical ensemble, the excess Gibbs free energy can be calculated from $G_{\rm ex} = n\langle\tilde{\mu}_{\rm ex}[w]\rangle$, with the ensemble average approximated by a time average using field configurations sampled in a field-theoretic simulation. Similarly, the excess Helmholtz free energy is obtained from $A_{\rm ex} = n\langle\tilde{\mu}_{\rm ex}[w]\rangle - \langle\tilde{P}_{\rm ex}[w]\rangle V$, involving both excess chemical potential and pressure field operators. Remarkably, these are direct operator averages that can be evaluated from data accumulated in a single simulation. Such operators have been used to conduct field-theoretic simulations of phase coexistence by matching pressures and chemical potentials (18) and via the Gibbs ensemble (19–21), but their utility in direct free energy evaluation has not been appreciated in the literature.

The restriction to purely repulsive interactions in the monatomic fluid example is readily overcome since any pair potential $u(r)$ that is finite at contact can be accurately decomposed into a sum of purely repulsive and purely attractive interactions using a basis set such as zero-centered Gaussians. Each successive term requires an additional auxiliary field to decouple the corresponding interaction (a real field for an attractive interaction and an imaginary field for a repulsion), but the structure of the field theory is otherwise unchanged. Long-ranged Coulomb interactions are similarly treated by introducing an auxiliary field $w_{el}(\mathbf{r})$ that can be interpreted as a fluctuating electrostatic potential (14, 18). The inverse Coulomb operator, corresponding to the first term in Eq. 3, results in a quasi-local square-gradient contribution to the Hamiltonian $\sim |\nabla w_{el}|^2$. Thus, the problematic long-range character of electrostatic interactions familiar in particle simulations (1) is avoided in a field-theoretic representation. While three-body (or higher-order) non-bonded potentials are not easily accommodated in the AF framework, they can in principle be included using a different coherent states (CS) representation discussed below (22).

Beyond atomic fluids, particle-based models of classical polymers are readily converted from coordinate to AF representations. For a one-component melt with polymer segments interacting via a purely repulsive non-bonded potential $u(r)$, the field-theoretic representation remains the same as Eqs. 2 and 3, but the functional $Q[iw]$ is now the partition function of a *single polymer* in the purely imaginary field $iw(\mathbf{r})$. Since a polymer is a one-dimensional chain of bonded segments, $Q[iw]$ can be efficiently computed for a prescribed field $w(\mathbf{r})$ by a transfer matrix approach (14).

Quantum fluids. Quantum many-body systems can also be given either a coordinate or field-theoretic representation. For a collection of n bosons in the canonical ensemble, the partition function can be expressed in a coordinate basis as (23)

$$\mathcal{Z}(n,V,T) = \frac{1}{n!}\sum_P \int dR\; \left\langle R\left|\exp(-\beta\hat{H})\right|\mathcal{P}R\right\rangle \qquad [5]$$

where R is a shorthand for the $3n$ particle coordinates in a three-dimensional volume V, $\hat{H}$ is the Hamiltonian operator, and the average over all $n!$ permutations P of particle labels with corresponding permutation operator $\mathcal{P}$ enforces Bose statistics. In Feynman's path integral framework (24), the object $\exp(-\tau\hat{H})$ is viewed as a many-body evolution operator in an "imaginary time" τ that is periodic with interval $[0,\beta]$. The imaginary-time particle trajectories included in Eq. 5 are closed cycles, analogous to classical ring polymers, and the terms in the permutation sum include primary cycles formed by individual particles and larger linked cycles formed by exchanging paths of two or more particles. The latter contribute exchange interactions. By performing a Trotter-Suzuki decomposition of the evolution operator (25), dividing the imaginary time interval $[0,\beta]$ into small increments, and inserting complete sets of intermediate coordinate states, a quantum theory is obtained that resembles a reactive ensemble of classical ring polymers. This is the basis for a particle-based simulation framework known as path integral Monte Carlo (PIMC) (26, 27). As in the classical partition function of Eq. 1, the n dependence in Eq. 5 cannot be isolated, so there is no simple chemical potential operator.

There is also a well established route to expressing an equilibrium quantum many-body system as a field theory. The method involves re-framing the problem in second quantization using a complete basis of abstract, single-particle occupation number states in which Bose or Fermi statistics are embedded (28). A subsequent Trotter-Suzuki decomposition of the density matrix using linear combinations of the occupation number states known as "coherent states" (CS) leads to an imaginary time, path integral representation of the partition function in field-theoretic form (29). For a fluid of particles satisfying Bose statistics, the canonical partition function can

$$S(\psi;[\phi^*,\phi]) = i\psi\, n + \int_0^\beta d\tau \int_V d^3r\; \phi^*(\mathbf{r},\tau+)\frac{\partial}{\partial\tau}\phi(\mathbf{r},\tau) + \int_0^\beta d\tau \int_V d^3r\; \phi^*(\mathbf{r},\tau+)\left[-\frac{\hbar^2\nabla^2}{2m} - i\psi\, k_BT\right]\phi(\mathbf{r},\tau) + \frac{1}{2}\int_0^\beta d\tau \int_V d^3r \int_V d^3r'\; \phi^*(\mathbf{r},\tau+)\phi^*(\mathbf{r}',\tau+)u(|\mathbf{r}-\mathbf{r}'|)\phi(\mathbf{r}',\tau)\phi(\mathbf{r},\tau) \quad [7]$$

be expressed as

$$\mathcal{Z}(n,V,T) = \int_{-\infty}^{\infty} d\psi \int \mathcal{D}(\phi^*,\phi)\; \exp\left[-S(\psi;[\phi^*,\phi])\right] \quad [6]$$

where S is an action functional given by Eq. 7. In this expression, ϕ and ϕ^* are complex-valued CS fields in the four-dimensional space of position $\mathbf{r}$ and imaginary time τ and are complex conjugates. They satisfy periodic boundary conditions in τ with period β; periodic conditions on $\mathbf{r}$ are also used in the bulk simulations reported here. The measure $\mathcal{D}(\phi^*,\phi)$ implies a functional integration over the real and imaginary parts of these two fields. The real variable ψ is a Lagrange multiplier to enforce a particle number of n, while m is the mass of a boson and $u(r)$ is the pair interaction potential. Finally, the notation $\tau+$ is a symbolic reminder that this expression relies on Itô stochastic calculus, so the ϕ^* field must be advanced in τ relative to ϕ when discretizing the τ variable (29).

As in the classical fluid case, the field-theoretic representation of the quantum fluid model isolates the number of particles n as a simple multiplicative factor in the action functional of Eq. 7. Application of the thermodynamic formula $\mu = (\partial A/\partial n)_{V,T}$ thus leads to $\beta\mu = \langle i\psi\rangle$, where the angle brackets represent an ensemble average over the ψ, ϕ, and ϕ^* variables with the *complex* statistical weight $\exp(-S)$. It follows that a chemical potential field operator for the theory is $\tilde{\mu}(\psi;[\phi^*,\phi]) = k_BT\, i\psi$, and the average of ψ must be a pure imaginary number. An expression for the pressure operator, $\tilde{P}(\psi;[\phi^*,\phi])$, is derived by a procedure similar to the classical fluid case and is given in Eq. S30 of the SI.

The classical and quantum field theory representations of Eqs. 2 and 6 provide immediate access to field operators that can be averaged to obtain Gibbs and Helmholtz free energies in the canonical ensemble, and by straightforward extension, the entropy in the microcanonical ensemble. Nonetheless, these representations come at a price: the Hamiltonian and action are complex-valued on the functional integration path. As a result, the field theories have a *sign problem* associated with non-positive-definite weights $\exp(-H)$ or $\exp(-S)$ that must be overcome when conducting numerical simulations. A versatile technique for circumventing this problem invokes a complex Langevin (CL) dynamics (30–32) that is the subject of the next section.

Models and Methods

Complex Langevin simulations. The CL method aims to develop a Markov chain of statistically important field configurations by integrating stochastic differential equations in a fictitious time θ. For a classical AF-type field theory, a suitable CL scheme is given by

$$\frac{\partial}{\partial\theta}w(\mathbf{r},\theta) = -\frac{\delta H[w]}{\delta w(\mathbf{r},\theta)} + \eta(\mathbf{r},\theta) \quad [8]$$

where $\eta(\mathbf{r},\theta)$ is a *real* Gaussian white noise whose statistical properties are defined by the moments $\langle\eta(\mathbf{r},\theta)\rangle = 0$ and $\langle\eta(\mathbf{r},\theta)\eta(\mathbf{r}',\theta')\rangle = 2\delta(\mathbf{r}-\mathbf{r}')\delta(\theta-\theta')$. Although the original integration path in Eq. 2 is restricted to the real axis, the Langevin dynamics of Eq. 8 explore complex-valued w configurations near constant-phase paths that pass through *saddle points* $w_s(\mathbf{r})$ of the model. These saddle points satisfy $\delta H/\delta w(\mathbf{r})|_{w_s} = 0$ and correspond to *mean-field* configurations. Indeed, with $\eta = 0$, Eq. 8 is a gradient-descent scheme for finding mean-field solutions (14). Access to mean-field solutions is an important advantage of the field-theoretic representation that we shall see also aids in free energy estimation.

If the stochastic dynamics of Eq. 8 produces a stationary distribution of complex states in the basin of a physically relevant saddle point, it can be proven that ensemble averages of the field theory can be computed as fictitious time averages along the stationary CL trajectory (33, 34). Thus, in a field-theoretic simulation conducted with CL sampling (FTS-CL), the average of a field operator $\tilde{G}[w]$ is obtained from the formula $\langle\tilde{G}[w]\rangle = (1/N_c)\sum_{l=1}^{N_c}\tilde{G}[w^l] + \mathcal{O}(N_c^{-1/2})$, where $w^l(\mathbf{r})$ are decorrelated states sampled at N_c discrete time points θ^l along the trajectory. Individual $\tilde{G}[w^l]$ values are complex, but the imaginary part of any physical field operator will vanish upon sufficient averaging. Although convergence to a steady state cannot be proved, we have found the FTS-CL method to be robust for the classes of models considered here. Nonetheless, failures of CL sampling have been documented in the literature (35–38). In some cases, "failure" can be attributed to the use of stochastic integration algorithms with poor stability characteristics. A more legitimate failure mode corresponds to a situation where a simulation remains stable, yet either the imaginary parts of physical operators do not average to zero or the highest Fourier modes of the fields fail to converge to a stationary distribution irrespective of the length of a simulation. Both are useful diagnostics of failure. We have observed such behavior in a few cases of fluid or polymer models with strong core repulsions.

A CL dynamics suitable for simulating the Bose fluid model of Eq. 6 evolves the scalar ψ variable by a dynamics similar to Eq. 8 and the ϕ and ϕ^* fields by an off-diagonal stochastic descent scheme (22, 39, 40),

$$\frac{\partial}{\partial\theta}\psi(\theta) = -\lambda\frac{\partial S(\psi;[\phi^*,\phi])}{\partial\psi(\theta)} + \eta_\psi(\theta) \quad [9]$$

$$\frac{\partial}{\partial\theta}\phi(\mathbf{r},\tau,\theta) = -\frac{\delta S(\psi;[\phi^*,\phi])}{\delta\phi^*(\mathbf{r},\tau,\theta)} + \eta(\mathbf{r},\tau,\theta)$$
$$\frac{\partial}{\partial\theta}\phi^*(\mathbf{r},\tau,\theta) = -\frac{\delta S(\psi;[\phi^*,\phi])}{\delta\phi(\mathbf{r},\tau,\theta)} + \eta^*(\mathbf{r},\tau,\theta) \qquad [10]$$

Here, $\lambda > 0$ is a real relaxation coefficient and η_ψ is a real Gaussian noise with vanishing mean and second moment $\langle\eta_\psi(\theta)\eta_\psi(\theta')\rangle = 2\lambda\,\delta(\theta-\theta')$. The noise sources in Eq. 10 are *complex conjugates* that can be expressed as $\eta = \eta_1 + i\eta_2$ and $\eta^* = \eta_1 - i\eta_2$, with η_1 and η_2 *real, independent* Gaussian noises. These have zero mean and covariance $\langle\eta_j(\mathbf{r},\tau,\theta)\eta_k(\mathbf{r}',\tau',\theta')\rangle = \delta_{j,k}\delta(\mathbf{r}-\mathbf{r}')\delta(\tau-\tau')\delta(\theta-\theta')$. While ϕ and ϕ^* are complex conjugates on the integration path of Eq. 6, this conjugacy is broken in the complex CL trajectories generated by Eq. 10 and both fields become independently complex. Similarly, the integration path of ψ is real in Eq. 6, but Eq. 9 explores complex ψ values.

Models. We illustrate the direct approach to free energy evaluation in the context of three models: a classical homopolymer solution, a melt of diblock copolymers, and the quantum Bose fluid model described by Eq. 6.

The *homopolymer solution model* is an implicit solvent model used by Edwards in analytical studies of excluded volume screening in polymer solutions (41, 42). We choose a non-bonded pair potential acting between polymer segments of the form $u(r) = u_0\varphi(r)$, where $\varphi(r) = 1/(8\pi^{3/2}a^3)\exp[-r^2/(4a^2)]$ is a repulsive Gaussian of range a normalized to have unit volume integral. The excluded volume parameter $u_0 > 0$ reflects the integrated potential strength and is the pseudo-potential coefficient in the contact interaction limit, $u(r) \to u_0\delta(\mathbf{r})$ for $a \to 0$. The field-theoretic representation of Eqs. 2 and 3 is applicable to the present model, but the single-chain partition function $Q[iw]$ remains to be specified. This functional is normalized by the partition function of a free (ideal) chain, so $Q[0] = 1$. Here we adopt the continuous Gaussian chain model (14, 43), corresponding to the continuum limit of a harmonic bead-spring chain. The partition function can be computed for a prescribed potential $w(\mathbf{r})$ as $Q[iw] = (1/V)\int_V d^3r\; q(\mathbf{r},N;[iw])$, where N is the contour length of the polymer, $q(\mathbf{r},s;[iw])$ is a chain propagator satisfying the modified diffusion equation

$$\frac{\partial}{\partial s}q(\mathbf{r},s;[iw]) = \left[\frac{b^2}{6}\nabla^2 - iw(\mathbf{r})\right]q(\mathbf{r},s;[iw]) \qquad [11]$$

and b is the statistical segment length. The propagator $q(\mathbf{r},s;[iw])$ represents the statistical weight for the end of a polymer chain of contour length s to be positioned at $\mathbf{r}$. Equation 11 is solved subject to the "initial" condition $q(\mathbf{r},0;[iw]) = 1$; i.e., a polymer of zero length is not influenced by the field $iw(\mathbf{r})$. Similar schemes have been devised for computing $Q[iw]$ for discrete bead-spring chain models with arbitrary bonded potentials (14). Finally, with lengths non-dimensionalized by the ideal chain radius-of-gyration $R_g \equiv b(N/6)^{1/2}$, all intensive thermodynamic properties of the homopolymer solution model are a function of three dimensionless parameters: a chain concentration $C \equiv nR_g^3/V$, an excluded volume strength $B \equiv \beta u_0 N^2/R_g^3$, and a non-bonded interaction range $\alpha \equiv a/R_g$.

The *diblock copolymer melt model* also employs continuous Gaussian chains, each chain consisting of an A block of Nf segments and a B block of $N(1-f)$ segments, f representing the mole/volume fraction of type A segments. We adopt equal statistical segment lengths $b_A = b_B = b$ for the two blocks and a non-bonded interaction of the form $\beta u(r) = \zeta v_0\varphi(r)$ between all pairs of segments, where v_0 is a reference segment volume, ζ is a dimensionless parameter that controls the compressibility of the melt, and $\varphi(r)$ is the same normalized Gaussian of range a used in the homopolymer model. Dissimilar pairs of A and B segments are subject to an additional interaction of the form $\beta u_{AB}(r) = \chi v_0\varphi(r)$, where χ is the dimensionless Flory interaction parameter (44). The limiting case of $\zeta \to \infty$, $a \to 0$ is the standard incompressible block copolymer model with contact interactions used in mean-field (self-consistent field theory, SCFT) calculations of copolymer phase behavior (45). Beyond SCFT, it is necessary to work with finite compressibility and interaction range to avoid ultraviolet divergences (16, 17).

The canonical partition function of the diblock model can be written in an AF form analogous to Eq. 2, but two fields are required to decouple the non-bonded interactions: $w_+(\mathbf{r})$ conjugate to the total segment density and $w_-(\mathbf{r})$ conjugate to the difference of A and B segment densities. Both fields are integrated along the real axis. The Hamiltonian functional is given by

$$H[w_\pm] = \frac{\rho_0}{2\zeta+\chi}\int_V d^3r\int_V d^3r'\; w_+(\mathbf{r})\varphi^{-1}(|\mathbf{r}-\mathbf{r}'|)w_+(\mathbf{r}')$$
$$+ \frac{\rho_0}{\chi}\int_V d^3r\int_V d^3r'\; w_-(\mathbf{r})\varphi^{-1}(|\mathbf{r}-\mathbf{r}'|)w_-(\mathbf{r}')$$
$$- n\ln Q[w_A,w_B] \qquad [12]$$

where $\rho_0 = 1/v_0$ is a reference segment density. The single copolymer partition function $Q[w_A,w_B]$ is again computed by solving Eq. 11, but with iw replaced by $w_A \equiv iw_+ - w_-$ for $0 \le s < Nf$ and by $w_B \equiv iw_+ + w_-$ for $Nf < s \le N$ (13, 14). The parameter v_0 should be viewed as a constant for the purpose of taking n or V derivatives to obtain chemical potential or pressure operators. However, a convenient value is the average volume per segment $v_0 = V/(nN)$. With this choice, the intensive thermodynamic properties of the diblock copolymer model are dictated by five dimensionless parameters: the block segregation strength χN, the A block fraction f, the chain concentration C, the melt compressibility parameter ζN, and the interaction range parameter α.

The *Bose fluid model* considered is described by Eqs. 6 and 7 with a pseudo-potential approximation for the pair potential, $u(r) = g\,\delta(\mathbf{r})$. The contact interaction volume g is related to the s-wave scattering length a_s by the expression $g = 4\pi\hbar^2 a_s/m$ and can be tuned in cold atom experiments by accessing Feshbach resonances (46). Convenient choices of length and energy scales for the model are given by $\lambda_r = 2mg/\hbar^2$ and $\lambda_E = (\hbar^2/2m)^3/g^2$, respectively. All intensive thermodynamic properties can thus be expressed in terms of the dimensionless temperature and density variables $\bar{T} \equiv k_BT/\lambda_E$, $\bar{\rho} \equiv n\lambda_r^3/V$.

Numerical methods. Field operations are conducted by spectral collocation with a uniform grid and plane wave basis (14, 47), including the imaginary time τ coordinate of the quantum theory. Periodic boundary conditions are imposed on the 3d simulation cell in space for the polymer models

and on the 4d cell in space and imaginary time for the Bose model. Spatial derivatives and convolutions are evaluated spectrally using discrete Fourier transforms. The imaginary time derivative in Eq. 7 is approximated by a first-order finite difference formula consistent with the causal properties of the theory (29, 40). Equation 11 is solved by a second-order Strang operator splitting algorithm (48, 49), stepping forward in s from the initial condition at $s = 0$ to the chain end at $s = N$. The functional derivatives in the CL equations 8 and 10 are formed analytically and the resulting force operators evaluated numerically on the computational grid. Equation 8 is stepped in fictitious time using a exponential time-differencing algorithm with weak first-order accuracy and excellent stability (ETD1) (16, 17). The CL equations 10 for the CS fields are time-stepped using a similar ETD1 algorithm (40). Equation 9 is integrated using an explicit Euler-Maruyama method of weak first-order accuracy (50).

All FTS-CL simulations were conducted using a custom C++ code base optimized for GPU parallelism on NVIDIA hardware.

Solid and liquid crystal mesophases. The direct method of free energy evaluation described in the introduction requires additional steps to relieve internal stress when simulating liquid crystalline or solid phases. Field-theoretic simulations are not applicable to atomistic models of molecular or polymer crystals because the harshly repulsive potentials in such models demand prohibitive levels of spatial resolution and CL sampling becomes difficult. However, surfactant molecules, liquid crystals, and block copolymers can form larger-scale periodic mesophases and be described by soft-core models for which field-theoretic simulation (FTS) is ideally suited (14). The diblock copolymer melt model considered here has six known ordered mesophases at the mean-field (SCFT) level: body-centered cubic spheres (BCC), face-centered cubic spheres (FCC), hexagonally-packed cylinders (HEX), lamellae (LAM), bicontinuous cubic double gyroid (GYR), and bicontinuous orthorhombic (O70) (51, 52). LAM and HEX are liquid-crystalline phases with at least one homogeneous direction in the unit cell; the remaining mesophases listed are solids.

In the case of a *liquid-crystalline mesophase*, a prerequisite to free energy evaluation is to relax the shape of the cell at fixed n and V until the average internal stress $\boldsymbol{\sigma}$ is isotropic and equal to $-P\mathbf{I}$ with $\mathbf{I}$ the unit tensor. This can be done manually (53), or automatically by an extension of the Parrinello-Ray-Rahman (PRR) framework (54, 55) to variable cell FTS (56). The necessary stress operator $\tilde{\boldsymbol{\sigma}}[w_\pm]$ is derived by a procedure analogous to that for the pressure operator and is provided in Eq. S28 of the SI. The final cell shape dictates the equilibrium domain spacing of a LAM or HEX phase (53, 57). Not recognized in prior work, however, is that the Helmholtz free energy can be directly computed as an operator average in the equilibrium cell by the formula $A = n\langle\tilde{\mu}[w_\pm]\rangle - \langle\tilde{P}[w_\pm]\rangle V$.

The case of a *solid mesophase* is more challenging. Relaxation of cell shape at fixed n and V will yield a cell with a residual isotropic stress because n and/or V are incompatible with an integer number of equilibrium unit cells of the mesophase. Instead, we consider cell shape and size variations of the *intensive* Helmholtz free energy at fixed chain concentration $c = n/V$. Specifically, we seek the equilibrium condition

$$\left.\frac{\partial[\beta A(n,\mathbf{h},T)/V]}{\partial\mathbf{h}}\right|_{c,T} = \left.\frac{\partial[\beta A_{\rm ex}(n,\mathbf{h},T)/V]}{\partial\mathbf{h}}\right|_{c,T} = 0 \quad [13]$$

where $\mathbf{h}$ is the cell tensor defining the shape and volume, $V = \det\mathbf{h}$, of a parallelepiped cell within the PRR framework (54–56). The first equality follows because the ideal gas contribution to $\beta A/V$ is constant at fixed c. It is shown in the SI that the requisite cell derivative can be written as

$$\left.\frac{\partial(\beta A_{\rm ex}/V)}{\partial\mathbf{h}}\right|_{c,T}\mathbf{h}^T = c\beta\langle\tilde{\mu}_{\rm ex}(\mathbf{h};[w_\pm])\rangle\,\mathbf{I} - (\beta A_{\rm ex}/V)\,\mathbf{I} + \beta\langle\tilde{\boldsymbol{\sigma}}_{\rm ex}(\mathbf{h};[w_\pm])\rangle \quad [14]$$

For a fluid or liquid crystal whose cell has been relaxed at fixed volume to a state of isotropic stress, $\langle\tilde{\boldsymbol{\sigma}}_{\rm ex}(\mathbf{h};[w_\pm])\rangle = -P_{\rm ex}\mathbf{I}$, the right hand side of Eq. 14 vanishes if the excess free energy is computed according to $A_{\rm ex} = n\langle\tilde{\mu}_{\rm ex}[w_\pm]\rangle - \langle\tilde{P}_{\rm ex}[w_\pm]\rangle V$. This validates our method of equilibrium domain spacing and free energy determination in the two cases.

For a solid mesophase, a multistep procedure is required. The first step is to find a cell configuration for which the average internal stress $\langle\tilde{\boldsymbol{\sigma}}_{\rm ex}\rangle$ is isotropic by relaxing in shape at constant volume (56). The resulting "reference" shape $\mathbf{h}_r$ is unlikely to satisfy the equilibrium condition (Eq. 13) because it will be improperly sized. We thus consider variations in cell volume at *fixed shape and chain concentration* via $\mathbf{h}(s) = s\,\mathbf{h}_r$, where s is a cell dilation/contraction parameter. Equation 14 then reduces to the linear differential equation

$$\frac{d}{d\ln s}\mathcal{A}(s) = \mathcal{F}(s) - \mathcal{A}(s) \quad [15]$$

where $\mathcal{A}(s) \equiv \beta A_{\rm ex}(s)/V$ is the free energy density in excess of the ideal gas and $\mathcal{F}(s) \equiv c\beta\langle\tilde{\mu}_{\rm ex}(\mathbf{h}(s);[w_\pm])\rangle - \beta\langle\tilde{P}_{\rm ex}(\mathbf{h}(s);[w_\pm])\rangle$ is the linear combination of operator averages that coincides with the free energy density at the equilibrium cell size s_0, $\mathcal{A}(s_0) = \mathcal{F}(s_0)$. Importantly, $\mathcal{F}(s)$ can be computed at any s by an FTS-CL simulation. We thus require a reference value of $\mathcal{A}$ in an isotropically-stressed cell to integrate Eq. 15 and establish where $\mathcal{A}(s)$ crosses $\mathcal{F}(s)$. In many cases the equilibrium cell size is well-approximated by its mean-field (SCFT) value $s_{0,SCFT}$, obtained as described in Ref. (56). This enables a direct estimate of the equilibrium free energy by means of $\mathcal{A}(s_0) \approx \mathcal{F}(s_{0,SCFT})$, the latter quantity evaluated by a single FTS-CL simulation in the mean-field cell. Alternatively, thermodynamic integration (17, 58) can be used to obtain a reference value of $\mathcal{A}$, e.g. $\mathcal{A}(s_{0,SCFT})$, from which Eq. 15 can be integrated to obtain a refined estimate of s_0 and $\mathcal{A}(s_0)$.

Results

Our first example of direct free energy evaluation is for the homopolymer solution model, which exhibits only a single homogeneous fluid phase. Figure 1 reports the intensive free energy in excess of the mean-field (SCFT) value, i.e. the fluctuation contribution, across five decades of dimensionless chain concentration C. A cubic cell of side length $L = 6.4\,R_g$ was employed and the non-bonded interaction strength and range were $B = 2$ and $\alpha = 0.2$, respectively. The filled circles are the result of the direct method, obtained by averaging chemical potential and pressure operators at the indicated value of C.

At one concentration we report the free energy obtained by thermodynamic integration (TI) from an Einstein crystal reference, a method developed in the context of particle simulations of solids (59, 60) and subsequently extended to field-theoretic simulations (17, 58). In a third approach, we applied TI from an ideal gas reference, integrating the average chemical potential according to $A_{\rm ex}/n = C^{-1}\int_0^C dC'\ \langle\tilde{\mu}_{\rm ex}[w]\rangle_{C',T}$. Gauss-Legendre quadrature was applied with 10 points across the $[0, C]$ interval. It is seen that all three methods based on FTS-CL yield consistent values, although the direct method provides the highest accuracy at an order-of-magnitude lower computational cost. The solid curve in the figure is an analytical reference obtained by expanding the Hamiltonian to quadratic order about the homogeneous saddle point and performing the resulting Gaussian functional integral (17). This "Gaussian approximation" is asymptotically exact for $C \to \infty$.

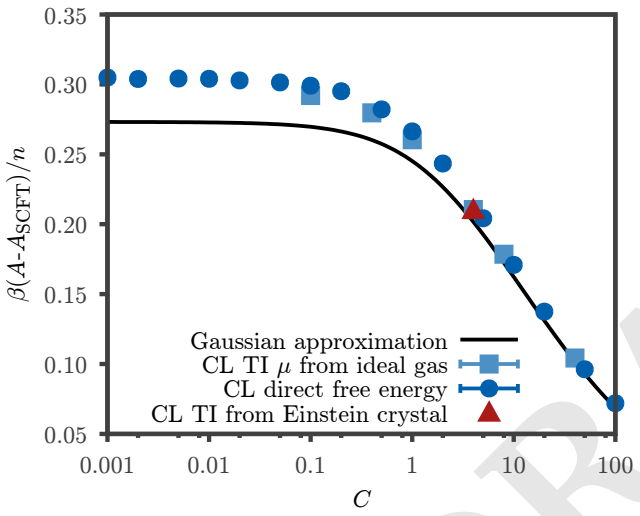

Fig. 1. Fluctuation contribution to the Helmholtz free energy per chain for the homopolymer solution model as a function of dimensionless chain concentration $C = nR_g^3/V$. Three free energy estimation methods were employed based on FTS-CL simulations: the direct method described here, thermodynamic integration of the chemical potential from the ideal gas reference, and thermodynamic integration from an Einstein crystal reference. The solid curve is a Gaussian approximation to the partition function integral that is asymptotic at large C.

As a second example, we illustrate the cell optimization used to determine the equilibrium domain spacing D_0 and free energy of a diblock copolymer melt in the lamellar (LAM) mesophase, an example of a liquid crystalline phase. If the phase is oriented with layer normals along the x axis, one can fix the lateral cell dimensions to a value $L = h_{yy} = h_{zz}$ much greater than the correlation length and then sweep $L_x = h_{xx}$ at fixed chain concentration C until the averages of the diagonal stress elements all agree. This procedure is demonstrated in Fig. 2 for the AB diblock copolymer model with parameters $\chi N = 20$, $f = 0.5$, $\alpha = 0.2$, and $\zeta N = 100$. Two periods of the stable lamellar phase were captured, oriented as described above. In panel (a), we see for the case of $C = 10$ that the three diagonal components of the average excess stress can be brought into agreement by adjusting L_x to approximately $8.69\ R_g$. Panel (b) shows how the optimal (single period) domain spacing D_0 obtained from this protocol using FTS-CL simulations varies with the dimensionless chain concentration C. As expected, D_0 approaches the value predicted from SCFT for $C \to \infty$, a limit in which mean-field theory is asymptotically exact (61). Nonetheless, for $C > 4$ we see that D_0 in a fluctuating system differs from the SCFT value by less than 0.4%. Remarkably, once the cell tensor $\mathbf{h}$ has been found that renders the stress isotropic, the free energy of the mesophase can be obtained by a simple averaging of chemical potential and pressure operators.

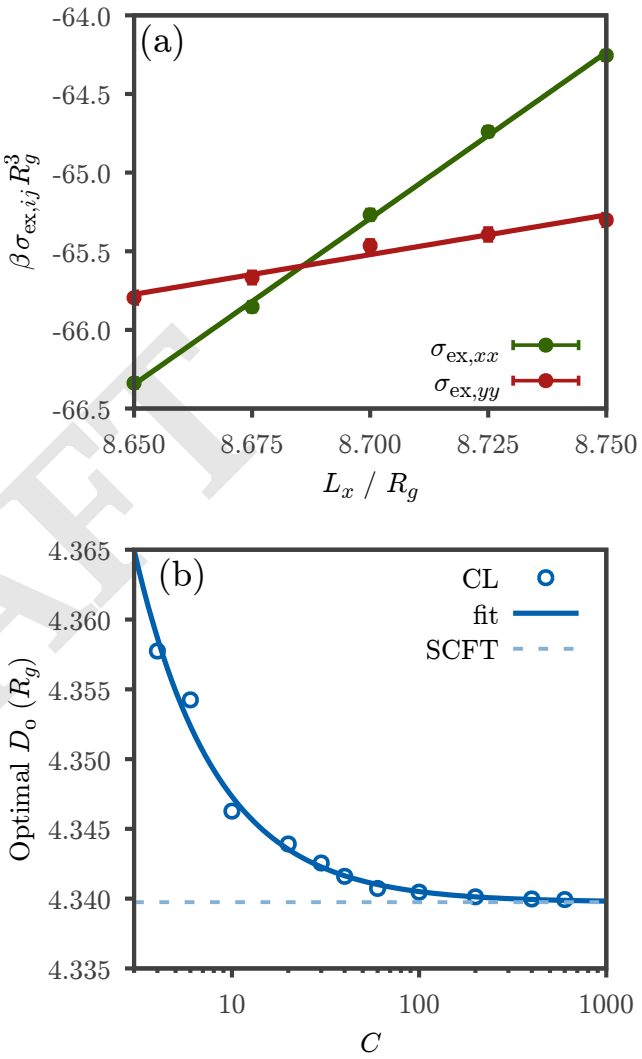

Fig. 2. Panel (a): Example of varying the cell dimension along the interface normal, $L_x = h_{xx}$, of two periods of the lamellar phase of a symmetric diblock copolymer while maintaining the chain concentration and cell dimensions $h_{yy} = h_{zz}$ in the transverse homogeneous directions constant. Under FTS-CL sampling, the average of the three principal stress components can be brought into agreement, determining the equilibrium cell size. Panel (b): The equilibrium FTS-CL domain spacing, D_0, approaches the SCFT prediction at large dimensionless chain concentrations C. The solid curve is a fit of the form $D_0 - D_{0,\rm SCFT} \sim C^{-1}$ to the simulation data. The lateral cell size is $L_y = L_z = 6.0\,R_g$ for all simulations.

Our third example of direct free energy evaluation is for a solid diblock copolymer mesophase, the bicontinuous double gyroid phase (GYR). At the value of dimensionless chain concentration chosen, $C = 7$, the cubic equilibrium cell configuration is well-approximated by the SCFT cell to better than 0.1%, so we make the approximation $s_0 \approx s_{0,SCFT}$ and

pre-compute the SCFT cell prior to estimating the free energy via the formula $\mathcal{A}(s_0) \approx \mathcal{F}(s_{0,SCFT})$ by an FTS-CL simulation. Results from this procedure are shown in Fig. 3, where the excess Helmholtz free energy per chain is reported for the GYR phase of the diblock copolymer melt model across a range of A-block fraction f. The model parameters are $\alpha = 0.25$, $\chi N = 16$, $\zeta N = 100$, and $C = 7$. We observe quantitative agreement between free energy predictions from the direct method and a method based on thermodynamic integration from an Einstein crystal reference (17, 58), also using the SCFT cubic cell. A significant fluctuation correction to the SCFT free energy is found in this case. The direct method yields results that are not only more accurate than those obtained by TI, but each data point requires only a single FTS-CL simulation and operator average, whereas greater than ten of those operations were needed to obtain each TI data point.

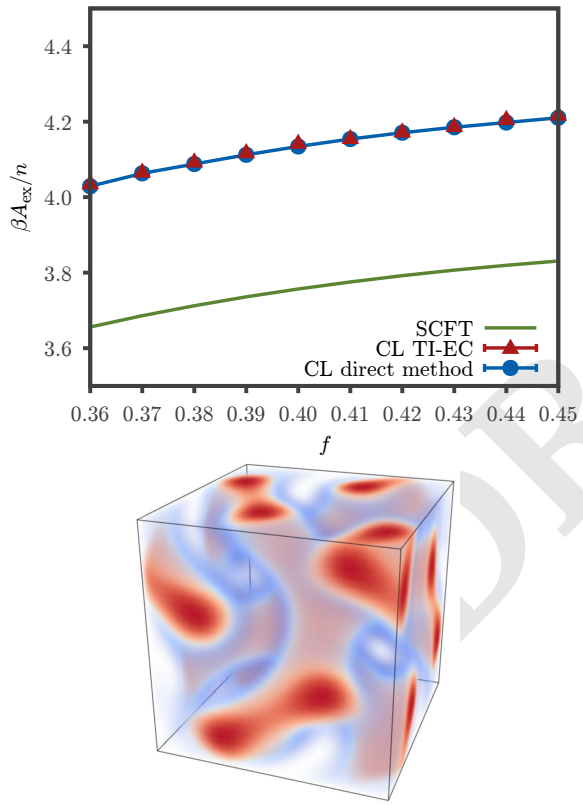

Fig. 3. (Top) Free energy comparison between the direct method (blue circles) and thermodynamic integration from an Einstein crystal reference (red triangles) in the equilibrium SCFT cell for a melt of diblock copolymers in the cubic double gyroid mesophase for various A-block fractions, f. The two methods are in quantitative agreement on the magnitude of fluctuation corrections from the SCFT free energy (green curve). (Bottom) 3D volumetric render of the A domain of the SCFT density for a single conventional cubic cell of the GYR phase at $f = 0.36$.

As a final example of direct free energy evaluation, we consider the Bose fluid model of Eqs. 6 and 7. For an ideal gas (Fig. 4, top panel), the Helmholtz free energy per particle is computed by the direct method of CL-averaging chemical potential and pressure operators given in the SI. The results

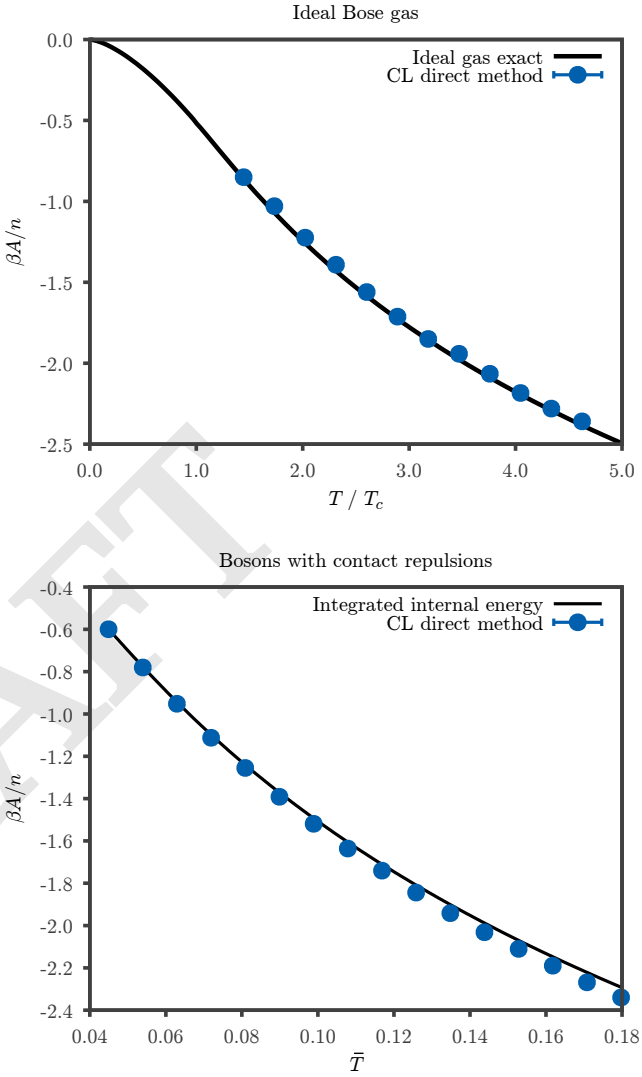

Fig. 4. (Top) Helmholtz free energy per particle of an ideal gas of bosons as a function of reduced temperature. Direct free energy calculations (blue circles) from complex Langevin simulations match the exact ideal gas result of Eq. 16 (black line). The CL simulations used 64 imaginary time samples and 16 spatial samples in each direction, the particle density was fixed at $n/V = 2.61$ in units of λ_c^{-3}, where λ_c is the thermal de Broglie wavelength at T_c, and the simulation cell size was set to $2.7\,\lambda_c$. (Bottom) For bosons with repulsive contact interactions, $g > 0$, the Helmholtz free energy per particle computed with the direct method is compared to the internal energy integrated over temperature using Eq. 17. The direct free energy estimate at the lowest temperature is used as a reference to align the integrated energy. The dimensionless particle density is $\bar{\rho} = 4.5 \times 10^{-4}$ and the simulation cell size is fixed at $2.65\,\lambda_r$. The action (Eq. 7) is discretized with 32 collocation mesh points in each spatial direction and 64 imaginary time slices.

are compared to an exact reference (28),

$$\frac{\beta A}{n} = \begin{cases} -\left(\frac{T}{T_c}\right)^{3/2} \frac{\zeta(5/2)}{\zeta(3/2)} & T < T_c \text{ BEC} \\ -\left(\frac{\mathrm{Li}_{5/2}(z)}{\mathrm{Li}_{3/2}(z)} + \ln z\right) & T > T_c \text{ normal fluid} \end{cases} \quad [16]$$

where $\mathrm{Li}_s(z)$ the polylogarithm function of order s, $\zeta(x)$ is the Riemann zeta function, z is the activity in the normal fluid equation of state $\mathrm{Li}_{3/2}(z) = n\lambda_T^3/V$, and T_c is the critical temperature where a Bose-Einstein condensate (BEC) appears.

For bosons with repulsive pair interactions, $g > 0$, an exact analytic reference is not available for the Helmholtz free energy. In this case, we use standard thermodynamic relations to compute a reference by integrating the temperature-dependent average internal energy,

$$\beta A\,(T) = \beta A\,(T_0) - \frac{1}{k_B}\int_{T_0}^{T} dT'\,(T')^{-2}\langle\widetilde{U}(T')\rangle \quad [17]$$

where $\widetilde{U}$ is an internal energy field operator whose form is given in Eq. S32 of the SI. In the bottom panel of Fig. 4, we use the lowest temperature as the reference T_0, integrate the internal energy by first fitting a cubic spline between CL estimates of $\beta\langle\widetilde{U}\rangle/T$, and use the direct method to determine $\beta A\,(T_0)$ for alignment of the integrated result to the same absolute reference. Again, excellent agreement is seen between free energies obtained by the direct method with reference values.

Discussion

We have presented a new "direct" approach to free energy evaluation that relies on the existence of a chemical potential field operator for many-body problems expressed in the canonical or microcanonical ensemble and framed in a field-theoretic representation. The method represents the most efficient technique for free energy evaluation within field-theoretic simulations, and for soft-core models normally studied in a coordinate representation, provides a new venue for free energy estimation by analytical conversion of the model to a field theory.

Beyond the ease and efficiency of free energy evaluation, field-theoretic simulations of classical systems have a number of advantages over traditional particle-based Monte Carlo and MD methods (1–3), including a computational cost that is nearly independent of density or polymer chain length (62), more straightforward and efficient treatment of long-range electrostatic interactions (18, 21, 63), and direct access to mean-field solutions for homogeneous and inhomogeneous systems that become increasingly accurate at high concentration (14).

In spite of these advantages, there are a number of barriers preventing the wide scale adoption of field-theoretic representations and simulation methods. An important limitation is that the techniques are relatively new and little open source software exists. The approach is also not suitable for atomic scale models with hard-core potentials. This restriction is not fatal, as methods such as variational coarse-graining (64) and relative entropy minimization (65) exist for mapping classical all-atom models to softer, coarse-grained models that are faithful to mesoscopic structure and thermodynamics. Moreover, soft-core models are a common starting point in soft matter simulations using tools such as dissipative particle dynamics (DPD) (66–68). Such models can be analytically converted to a field theory, allowing for efficient phase diagram construction via SCFT or FTS-CL (69), the latter utilizing the free energy method presented here. Nonetheless, the extra step of coarse-graining represents a barrier if the starting model is atomistic.

For quantum many-body systems, the most significant limitation is that the approach advocated here is inapplicable to particles with Fermi statistics. The CS representation in this case involves integrals over fields satisfying Grassmann algebra, rather than conventional Riemann integrals in the Bose CS case. While an AF representation is possible, the action is plagued with branch point singularities associated with zeros of the fermion determinant (29, 70), which defy CL sampling. Fortunately, there are many interesting continuum and lattice problems involving Bose statistics that can be tackled with FTS-CL and the present free energy method, including some with sign problems that do not succumb to existing quantum Monte Carlo algorithms.

An important advantage of the present method is that it enables a "pointwise" estimate of the free energy at specified model parameters by averaging operators within a single simulation. Flat histogram approaches such as the Wang-Landau method (10), its extension to quantum Monte Carlo (12), and the closely related metadynamics (71) must perform a random walk in some collective coordinate (e.g. energy) to converge and gain statistics. The diffusive timescale (and hence computational effort) of the latter methods grows approximately as the square of both the coordinate range and the number of particles (72). Conversely, the timescale to equilibrate a field-theoretic simulation and obtain a pointwise free energy estimate is *independent* of the particle number n (at constant V). Flat histogram algorithms are also complicated to implement and to prove convergence, especially in the quantum case. They have found limited utility in mapping liquid-solid and solid-solid phase boundaries, notably surfactant and polymer systems with multiple liquid crystalline and/or solid mesophases.

The most compelling case for the field-theoretic approach currently involves dense assemblies of long polymers, particularly charged polymers and self-assembling systems such as block copolymers, but we expect similar examples to be found in Bose quantum systems at high density and low temperature.

ACKNOWLEDGMENTS. The authors are grateful to M. S. Shell for helpful discussions. This work was supported by the Condensed Matter and Materials Theory Program of the National Science Foundation (NSF), Award No. DMR-2104255. Use was made of computational facilities purchased with funds from the NSF (OAC-1925717) and administered by the Center for Scientific Computing (CSC). The CSC is supported by the California NanoSystems Institute and the NSF MRSEC (DMR-1720256) at UC Santa Barbara.

1. D Frenkel, B Smit, *Understanding molecular simulation.* (Academic Press, London), (1996).
2. MP Allen, DJ Tildesley, *Computer Simulation of Liquids.* (Oxford University Press, New York), (1987).
3. DP Landau, K Binder, *A Guide to Monte Carlo Simulation in Statistical Physics.* (Cambridge University Press, Cambridge), (2000).
4. MS Shell, A Panagiotopoulos, A Pohorille, Methods Based on Probability Distributions and Histograms in *Springer Ser. Chem. Phys.*, eds. C Chipot, A Pohorille. (Springer, Berlin) Vol. 86, pp. 77–118 (2007).
5. B Widom, Some Topics in the Theory of Fluids. *J. Chem. Phys.* **39**, 2808–2812 (1963).
6. J Batoulis, K Kremer, Statistical properties of biased sampling methods for long polymer chains. *J. Phys. A. Math. Gen.* **21**, 127–146 (1988).
7. D Frenkel, GCAM Mooij, B Smit, Novel scheme to study structural and thermal properties of continuously deformable molecules. *J. Phys. Condens. Matter* **4**, 3053–3076 (1992).
8. D Frenkel, B Smit, Unexpected length dependence of the solubility of chain molecules. *Mol. Phys.* **75**, 983–988 (1992).

9. JJ de Pablo, M Laso, UW Suter, Estimation of the chemical potential of chain molecules by simulation. *J. Chem. Phys.* **96**, 6157–6162 (1992).
10. F Wang, DP Landau, Efficient, Multiple-Range Random Walk Algorithm to Calculate the Density of States. *Phys. Rev. Lett.* **86**, 2050–2053 (2001).
11. NA Mahynski, et al., Flat-histogram extrapolation as a useful tool in the age of big data. *Mol. Simul.* **47**, 395–407 (2021).
12. M Troyer, S Wessel, F Alet, Flat Histogram Methods for Quantum Systems: Algorithms to Overcome Tunneling Problems and Calculate the Free Energy. *Phys. Rev. Lett.* **90**, 4 (2003).
13. GH Fredrickson, V Ganesan, F Drolet, Field-Theoretic Computer Simulation Methods for Polymers and Complex Fluids. *Macromolecules* **35**, 16–39 (2002).
14. GH Fredrickson, *The Equilibrium Theory of Inhomogeneous Polymers*. (Oxford University Press, Oxford), (2006).
15. D Chandler, *Introduction to Modern Statistical Mechanics*. (Oxford University Press, Oxford), (1987).
16. MC Villet, GH Fredrickson, Efficient field-theoretic simulation of polymer solutions. *J. Chem. Phys.* **141**, 224115 (2014).
17. KT Delaney, GH Fredrickson, Recent Developments in Fully Fluctuating Field-Theoretic Simulations of Polymer Melts and Solutions. *J. Phys. Chem. B* **120**, 7615–7634 (2016).
18. KT Delaney, GH Fredrickson, Theory of polyelectrolyte complexation—Complex coacervates are self-coacervates. *J. Chem. Phys.* **146**, 224902 (2017).
19. AZ Panagiotopoulos, Direct determination of phase coexistence properties of fluids by Monte Carlo simulation in a new ensemble. *Mol. Phys.* **61**, 813–826 (1987).
20. RA Riggleman, GH Fredrickson, Field-theoretic simulations in the Gibbs ensemble. *J. Chem. Phys.* **132**, 024104 (2010).
21. J McCarty, KT Delaney, SPO Danielsen, GH Fredrickson, JE Shea, Complete Phase Diagram for Liquid–Liquid Phase Separation of Intrinsically Disordered Proteins. *J. Phys. Chem. Lett.* **10**, 1644–1652 (2019).
22. X Man, KT Delaney, MC Villet, H Orland, GH Fredrickson, Coherent states formulation of polymer field theory. *J. Chem. Phys.* **140**, 024905 (2014).
23. RP Feynman, *Statistical Mechanics: A Set of Lectures*. (Addison-Wesley, New York), (1972).
24. RP Feynman, AR Hibbs, *Quantum Mechanics and Path Integrals*. (McGraw-Hill, New York), (1965).
25. M Suzuki, Relationship between d-Dimensional Quantal Spin Systems and (d+ 1)-Dimensional Ising Systems. *Prog. Theor.* **56**, 1454 (1976).
26. DM Ceperley, Path integrals in the theory of condensed helium. *Rev. Mod. Phys.* **67**, 279–355 (1995).
27. M Boninsegni, N Prokof'ev, B Svistunov, Worm Algorithm for Continuous-Space Path Integral Monte Carlo Simulations. *Phys. Rev. Lett.* **96**, 070601 (2006).
28. AL Fetter, JD Walecka, *Quantum Theory of Many-Particle Systems*. (McGraw-Hill, New York), (1971).
29. JW Negele, H Orland, *Quantum Many-particle Systems (Advanced Books Classics)*. (Addison-Wesley, New York), (1988).
30. G Parisi, Ys Wu, Perturbation Theory Without Gauge Fixing. *Sci. Sin.* **24**, 483 (1980).
31. G Parisi, On complex probabilities. *Phys. Lett. B* **131**, 393–395 (1983).
32. JR Klauder, A Langevin approach to fermion and quantum spin correlation functions. *J. Phys. A Math. Gen* **16**, 317–319 (1983).
33. WJ Schoenmaker, Monte Carlo simulations and complex actions. *Phys. Rev. D* **36**, 1859–1867 (1987).
34. S Lee, The convergence of complex Langevin simulations. *Nucl. Phys. B* **413**, 827–848 (1994).
35. G Aarts, E Seiler, IO Stamatescu, Complex Langevin method: When can it be trusted? *Phys. Rev. D* **81**, 054508 (2010).
36. G Aarts, et al., Stability of complex Langevin dynamics in effective models. *J. High Energy Phys.* **2013**, 73 (2013).
37. M Scherzer, E Seiler, D Sexty, IO Stamatescu, Complex Langevin and boundary terms. *Phys. Rev. D* **99**, 014512 (2019).
38. D Nilsson, B Bozorg, S Mohanty, B Söderberg, A Irbäck, Limitations of field-theory simulation for exploring phase separation: The role of repulsion in a lattice protein model. *J. Chem. Phys.* **156**, 015101 (2022).
39. G Aarts, Can Stochastic Quantization Evade the Sign Problem? The Relativistic Bose Gas at Finite Chemical Potential. *Phys. Rev. Lett.* **102**, 131601 (2009).
40. KT Delaney, H Orland, GH Fredrickson, Numerical Simulation of Finite-Temperature Field Theory for Interacting Bosons. *Phys. Rev. Lett.* **124**, 070601 (2020).
41. SF Edwards, The statistical mechanics of polymers with excluded volume. *Proc. Phys. Soc.* **85**, 613–624 (1965).
42. SF Edwards, The theory of polymer solutions at intermediate concentration. *Proc. Phys. Soc.* **88**, 265–280 (1966).
43. M Doi, SF Edwards, *The Theory of Polymer Dynamics*. (Oxford University Press, Oxford), (1986).
44. PG de Gennes, *Scaling Concepts in Polymer Physics*. (Cornell University Press, Ithaca), (1979).
45. MW Matsen, M Schick, Stable and unstable phases of a diblock copolymer melt. *Phys. Rev. Lett.* **72**, 2660–2663 (1994).
46. C Chin, R Grimm, P Julienne, E Tiesinga, Feshbach resonances in ultracold gases. *Rev. Mod. Phys.* **82**, 1225–1286 (2010).
47. D Gottlieb, SA Orszag, *Numerical Analysis of Spectral Methods*. (Society for Industrial and Applied Mathematics (SIAM), Philadelphia), (1977).
48. KØ Rasmussen, G Kalosakas, Improved numerical algorithm for exploring block copolymer mesophases. *J. Polym. Sci. Part B Polym. Phys.* **40**, 1777–1783 (2002).
49. G Tzeremes, KØ Rasmussen, T Lookman, A Saxena, Efficient computation of the structural phase behavior of block copolymers. *Phys. Rev. E* **65**, 041806 (2002).
50. PE Kloeden, E Platen, *Numerical Solution of Stochastic Differential Equations*. (Springer-Verlag, Berlin), (1999).
51. CA Tyler, DC Morse, Orthorhombic Fddd Network in Triblock and Diblock Copolymer Melts. *Phys. Rev. Lett.* **94**, 208302 (2005).
52. MW Matsen, Effect of Architecture on the Phase Behavior of AB-Type Block Copolymer Melts. *Macromolecules* **45**, 2161–2165 (2012).
53. B Vorselaars, P Stasiak, MW Matsen, Field-Theoretic Simulation of Block Copolymers at Experimentally Relevant Molecular Weights. *Macromolecules* **48**, 9071–9080 (2015).
54. M Parrinello, A Rahman, Polymorphic transitions in single crystals: A new molecular dynamics method. *J. Appl. Phys.* **52**, 7182–7190 (1981).
55. JR Ray, A Rahman, Statistical ensembles and molecular dynamics studies of anisotropic solids. *J. Chem. Phys.* **80**, 4423–4428 (1984).
56. JL Barrat, GH Fredrickson, SW Sides, Introducing Variable Cell Shape Methods in Field Theory Simulations of Polymers. *J. Phys. Chem. B* **109**, 6694–6700 (2005).
57. RKW Spencer, B Vorselaars, MW Matsen, Continuous Thermodynamic Integration in Field-Theoretic Simulations of Structured Polymers. *Macromol. Theory Simulations* **26**, 1700036 (2017).
58. EM Lennon, K Katsov, GH Fredrickson, Free Energy Evaluation in Field-Theoretic Polymer Simulations. *Phys. Rev. Lett.* **101**, 138302 (2008).
59. JQ Broughton, GH Gilmer, Molecular dynamics investigation of the crystal–fluid interface. I. Bulk properties. *J. Chem. Phys.* **79**, 5095–5104 (1983).
60. D Frenkel, AJC Ladd, New Monte Carlo method to compute the free energy of arbitrary solids. Application to the fcc and hcp phases of hard spheres. *J. Chem. Phys.* **81**, 3188–3193 (1984).
61. GH Fredrickson, E Helfand, Fluctuation effects in the theory of microphase separation in block copolymers. *J. Chem. Phys.* **87**, 697–705 (1987).
62. GH Fredrickson, KT Delaney, Field-theoretic simulations: An emerging tool for probing soft material assembly. *MRS Bull.* **43**, 371–378 (2018).
63. J Lee, YO Popov, GH Fredrickson, Complex coacervation: A field theoretic simulation study of polyelectrolyte complexation. *J. Chem. Phys.* **128**, 224908 (2008).
64. WG Noid, et al., The multiscale coarse-graining method. I. A rigorous bridge between atomistic and coarse-grained models. *J. Chem. Phys.* **128**, 244114 (2008).
65. MS Shell, The relative entropy is fundamental to multiscale and inverse thermodynamic problems. *J. Chem. Phys.* **129**, 144108 (2008).
66. PJ Hoogerbrugge, JMVA Koelman, Simulating Microscopic Hydrodynamic Phenomena with Dissipative Particle Dynamics. *Eur. Lett.* **19**, 155–160 (1992).
67. P Español, P Warren, Statistical Mechanics of Dissipative Particle Dynamics. *Eur. Lett.* **30**, 191–196 (1995).
68. RD Groot, PB Warren, Dissipative particle dynamics: Bridging the gap between atomistic and mesoscopic simulation. *J. Chem. Phys.* **107**, 4423–4435 (1997).
69. N Sherck, et al., Molecularly Informed Field Theories from Bottom-up Coarse-Graining. *ACS Macro Lett.* **10**, 576–583 (2021).
70. DJ Scalapino, RL Sugar, Method for Performing Monte Carlo Calculations for Systems with Fermions. *Phys. Rev. Lett.* **46**, 519–521 (1981).
71. A Laio, M Parrinello, Escaping free-energy minima. *Proc. Natl. Acad. Sci.* **99**, 12562–12566 (2002).
72. MS Shell, PG Debenedetti, AZ Panagiotopoulos, Flat-Histogram Dynamics and Optimization in Density of States Simulations of Fluids. *J. Phys. Chem. B* **108**, 19748–19755 (2004).